



High-resolution temperature observations of a trapped nonlinear diurnal tide influencing cold-water corals on the Logachev mounds



Hans van Haren*, Furu Mienis, Gerard C.A. Duineveld, Marc S.S. Lavaleye

Royal Netherlands Institute for Sea Research (NIOZ), P.O. Box 59, 1790 AB Den Burg, The Netherlands

ARTICLE INFO

Article history:

Received 15 November 2013

Received in revised form 16 April 2014

Accepted 20 April 2014

Available online 29 April 2014

ABSTRACT

A high-resolution thermistor string mooring of 120 m length was used to measure turbulence processes in the water layer above the foot of a densely populated cold-water coral mound at 919 m depth at the southeast slope of Rockall Bank in the Logachev area, North-East Atlantic Ocean. As expected from previous current observations, the temperature data reveal a dominant diurnal (tidal) periodicity associated with topography-trapped, weakly bottom-intensified waves. These baroclinic diurnal waves are driven to (near-) resonance around the mound and have vertical amplitudes exceeding the mooring line. Their horizontal excursion length matches the size of the mound, which causes a residual current around and flux up the mound. As their particle velocities also match the phase speed of the wave traveling around the mound, these waves can become highly nonlinear and show largest turbulence due to wave-breaking at the transition from warming downslope to cooling upslope tidal phase. Averaged over the entire 9-day time series and the 120 m vertical range, mean turbulent kinetic energy dissipation amounts to $2.2 \pm 1.1 \times 10^{-7} \text{ W kg}^{-1}$ (and mean vertical eddy diffusivity to $9 \pm 5 \times 10^{-3} \text{ m}^2 \text{ s}^{-1}$) with short-term variations over four orders of magnitude. Such large turbulence, more than 100 times larger than open-ocean values and comparable with that observed in tidally energetic shelf break-shallow sea areas, will affect the nutrient replenishment of the cold-water corals.

© 2014 Elsevier Ltd. All rights reserved.

Introduction

During the past decades research has shown that cold-water coral (CWC) ecosystems are widely distributed along the margins of the Atlantic Ocean, at depths between about 200 and 1000 m (e.g., Wheeler et al., 2007). These ecosystems are hotspots of biodiversity and carbon cycling (Henry and Roberts, 2007; van Oevelen et al., 2009). CWC can occur as solitary colonies, but can also form large reef or mound structures (De Mol et al., 2002; Lindberg et al., 2007). Such CWC reefs can be compared with a forest, forming a refuge, nursery and stable substrate for a lot of different associated species (Freiwald, 2003).

CWCs preferentially live in areas with periodically varying currents with relatively high speeds, varying between 0.1 and 0.15 m s^{-1} (Duineveld et al., 2007) to $>0.5 \text{ m s}^{-1}$ (Mienis et al., 2007; Dorschel et al., 2007). Such speeds increase the food supply and prevent the corals from burial by sediments (Frederiksen et al., 1992). For example in the NE Atlantic Ocean, bottom intensified semi-diurnal and diurnal tidal currents are associated with CWC-mounds over slopes of Porcupine and Rockall Banks (Duineveld

et al., 2007; Mienis et al., 2007; White et al., 2007), while the Mingulay reef complex is influenced by an internal hydraulic jump (Davies et al., 2009). Food web analyses of a CWC area on the southwest Rockall Trough margin have shown that corals mainly thrive on fresh phytodetritus (Duineveld et al., 2007). It is assumed that the dense coral framework acts as a sediment trap, which results in local accumulation of particles from the reef itself, and from the vertical flux of organic matter (Mienis et al., 2009). If coral growth outpaces sedimentation, a mound or reef structure will develop.

On the southeast slopes of Rockall Bank in the Logachev area (Fig. 1), dense living CWC covered carbonate mounds up to 360 m high are arranged in elongated clusters of several kilometers long and wide. Most mound clusters have an orientation which is slightly oblique to the large-scale depth contours (De Mol et al., 2002; van Weering et al., 2003; Kenyon et al., 2003; Mienis et al., 2006). The mounds occur in a narrow zone on the sloping margin between 600 and 1000 m water-depth. According to White et al. (2007), this depth-range roughly corresponds with depths where bottom-intensified diurnal tidal motions are present. It has been suggested that the diurnal tidal motion which brings alternating pulses of relatively cold and warm waters on the mounds, is important for coral growth, especially since the latter brings nutritious (fluorescent) material to the corals (Duineveld et al., 2007). White

* Corresponding author. Tel.: +31 222369300/369451.

E-mail address: hans.van.haren@nioz.nl (H. van Haren).

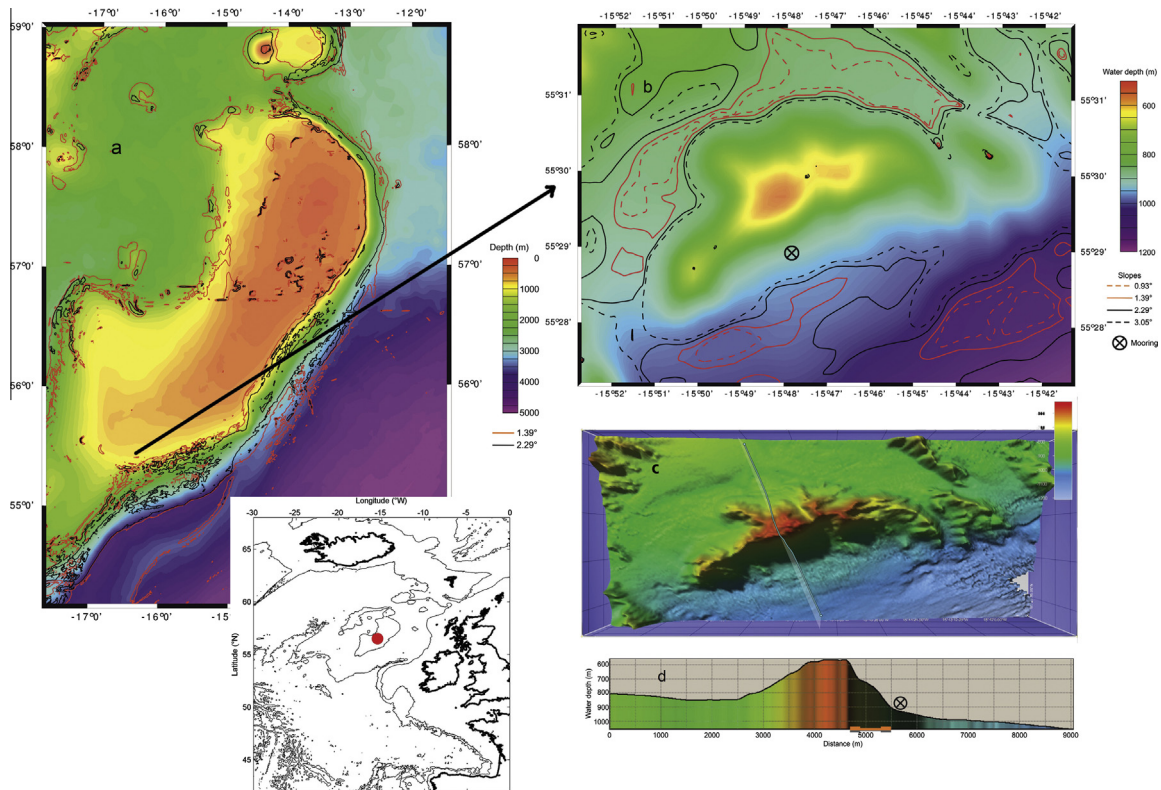


Fig. 1. Investigation area in the NE Atlantic Ocean. (a) Rockall Bank area, West of Ireland. Map based on half-minute GEBCO-data linearly interpolated to 500×500 m grid (note that this coarse sampling does not detect CWC-mounds properly); UTM-projection using reference-ellipsoid WGS84. Contours indicate slopes computed following (the inverse of) (1) using mean buoyancy frequency $N = 3 \times 10^{-3} \text{ s}^{-1}$, for diurnal (red) and inertial (black) frequencies. (b) Zoom of the Logachev cold-water coral mound area using 250×250 m grid Multibeam data, same projection as but different colour scheme than in a. The position of thermistor string/ADCP mooring is indicated by the encircled cross. The dashed contours are for extended range-values of N -1std = $2 \times 10^{-3} \text{ s}^{-1}$ (black dashed inertial frequency) and $N + 1 \text{ std} = 4 \times 10^{-3} \text{ s}^{-1}$ (red dashed diurnal frequency). (c) Original $\sim 15 \times 30$ m resolution Multibeam data for the area of b with the line indicating a cross-mound transect. (d) Cross-mound transect passing the mooring at 919 m to the right of mound. Most dense CWC-colonies (orange bar) occur on this side of the mound, with densest populations (densest orange) at the steepest slopes. (For interpretation of the references to colour in this figure legend, the reader is referred to the web version of this article.)

and Dorschel (2010) suggest a relation between the permanent thermocline and the depth range where mounds occur. It is further suggested by White et al. (2007) that the orientation of the mound clusters is modified by currents. In several areas the mounds are cross-slope oriented corresponding with the orientation of the local major axis of tidal current ellipses. However, uncertainties remain about the physical processes governing CWC growth on the Rockall Bank-mounds.

Here, we seek to quantify the process of turbulence induced via baroclinic wave breaking near a Logachev CWC-mound, southeast Rockall Bank. We not only expect enhanced tidal wave motions to shape the mounds' orientation, but also to influence the nutrient replenishment of the CWC. The quantification is done via analysis of data from a short-duration mooring with a string of high sampling-rate thermistors that was deployed downslope of a CWC-mound for 9 days in October 2012 as part of a larger program on CWC-behavior including extensive bottom investigations. Supporting moored acoustic current measurements and shipborne CTD-observations are used from nearby stations. Before presenting the observations, we first review some physical processes around Rockall Bank.

Potentially relevant tidal processes

As the Rockall Bank area is dominated by tides and particular diurnal tidal enhancement (Huthnance, 1974; Pingree and Griffiths, 1984; White et al., 2007), these periodic motions should be contained in the relevant physical processes. Throughout the region, surface tides are predominantly semidiurnal. However,

along the slopes of the Bank currents are diurnal. This remarkable difference has been observed around several islands along the West-Scotland coast (Moray, 1665; Cartwright, 1969). We distinguish several potential processes for the entire Rockall Bank and for the smaller-scale mound area on its southeastern slope.

First, the scales of the Rockall Bank (dimensions of about 300×150 km horizontally; Fig. 1a) drive the linear sub-inertial (frequencies $\sigma < f$, f denoting the inertial frequency), diurnal barotropic (vertically independent) tidal current to resonance (Huthnance, 1974). These currents result from the diurnal tidal wave being trapped by the topography (Longuet-Higgins, 1968). They are amplified by a factor of about five with respect to those of the surroundings and with respect to semidiurnal tidal currents. Cartwright (1969) observed that especially the near-solar diurnal tidal constituent K_1 is (resonantly) enhanced, but O_1 not. Later observations on resonant topographic diurnal tidal currents from other areas confirm this (e.g., Crawford and Thomson, 1982; Foldvik et al., 1990; Lam, 1999). In the analytic model for Rockall Bank employed by Huthnance (1974), this near-resonance is found for the lowest mode in radial direction. A numerical model by Pingree and Griffiths (1984) shows trapping for diurnal tidal currents with wave lengths of about 300 km, fitting the length of Rockall Bank. In their model, the enhanced horizontal currents (particle velocities) are found over the Bank, for water depths < 1000 m, and have amplitudes of about 0.1 m s^{-1} . As these currents are driven by the surface tidal slope, we expect zero phase-shift in observations made in the vertical. However, if the tidal current ellipses are not degenerate (rectilinear), the component perpendicular to the slope is expected to move ('slosh')

water up and down the slopes including the CWC-mound area. This implies moving waters have different temperature (density) across the mounds, under stable vertical density stratified conditions.

Second, the stratification allows for a type of wave associated with smaller scales around Rockall Bank. The physical phenomenon of near-bottom ‘trapping’ of density-gradient driven (baroclinic; vertically varying) waves is expected to lead to amplified motions when the frequency of the waves amounts, for an infinitely long slope (Rhines, 1970),

$$\sigma \leq N \sin \gamma, \quad (1a)$$

where N denotes the buoyancy frequency and γ the bottom slope. Depending on the parameter $S = N/f$, weak (for $S \sim 1$) or strong (for $S \gg 1$) amplitude dependence with depth is predicted. However, trapping does not imply wave amplitude enhancement with respect to the environment, like under resonant conditions.

As internal (inertio-gravity) waves can freely propagate when they have a frequency in the range $f \leq \sigma \leq N$ when $N \gg f$, topographic trapping will not occur for frequency range (1a) at the edge of a finite length of slope in a fluid bounded by a surface, like in the setting of a submarine bank. However, motions which have frequencies $\sigma < f$ may become ‘double trapped’, whereby they stay near their generation depths around a bank (Longuet-Higgins, 1968). This leads to an extra condition,

$$\sigma \leq N \sin \gamma < f, \quad (1b)$$

for bottom-trapped baroclinic waves. Using computed and observed parameters f and N for Rockall Bank, White et al. (2007) expected trapping for diurnal tidal frequencies to occur between about 700 and 1100 m. It is noted that these sub-inertial baroclinic waves are not standing waves; they propagate along the sloping topography with the shallow water to the right. This is the same direction as for the barotropic resonant waves trapped over Rockall Bank, modeled by Huthnance (1974) and Pingree and Griffiths (1984).

Third, the process of diurnal tidal amplification is entirely different from the process of free propagating semidiurnal internal tidal wave enhancement upon ‘critical reflection’, when the internal wave slope,

$$\beta = \sin^{-1}((\sigma^2 - f^2)^{1/2} / (N^2 - f^2)^{1/2}), \quad (2)$$

equals bottom-slope γ . This critical reflection has been proposed to be the dominant mechanism for sediment resuspension by various authors (e.g., Cacchione and Wunsch, 1974; Cacchione and Drake, 1986; Dickson and McCave, 1986; van Raaphorst et al., 2001). Comparing Eqs. (1) and (2) for the Rockall Bank area, we note that coincidentally and easy to proof for given stratification and latitude, one finds $\beta(M_2) \approx \sin^{-1}(\sigma(K_1)/N)$, to within the error of variation in mean $N \approx 25f$, for semidiurnal lunar tidal constituent M_2 and diurnal (\sim solar) constituent K_1 . As result, we cannot distinguish between critical semidiurnal internal tide reflection and diurnal baroclinic bottom trapping using observations of bottom topography and stratification only. The distinction between these processes should be revealed using moored observations.

Fourth, on horizontal scales of a 5×3 km CWC-mound, one may expect resonance of baroclinic motions, similar to Huthnance’s (1974) model for resonant barotropic motions around the entire Rockall Bank. If baroclinic wave resonance is sought in the circum-mound direction, a lowest mode baroclinic diurnal tide should have a phase speed of $c \approx 0.15 \text{ m s}^{-1}$ to fit one wavelength around the mound’s perimeter. Such a resonance condition may be applicable to bottom-trapped baroclinic motions, which in that case may have amplitudes much larger than those of their surroundings.

Fifth, in contrast with the above resonant barotropic linear waves, these baroclinic resonant or trapped waves are likely to

become highly nonlinear (Rhines, 1977). A simple condition for nonlinearity is the correspondence $|\mathbf{U}| = c$, where \mathbf{U} denotes the particle velocity (current speed). This condition is unlikely to be found for barotropic waves (Pingree and Griffiths, 1984) of estimated diurnal tidal phase speed $c = 3.5 \text{ m s}^{-1} \gg |\mathbf{U}| \approx 0.1 \text{ m s}^{-1}$. In contrast, the CWC-mound-scale $\approx NH/f = R$ the internal Rossby radius, with H the water depth, allows for near-resonant baroclinic conditions of $c \approx |\mathbf{U}|$. Indeed, frontal bores and highly non-linear internal waves occurring at sub-inertial (\sim several days) periodicities have been observed along various topography, in a lake near the surface (Thorpe et al., 1996) and in the Faeroe-Shetland Channel above the bottom (Hosegood et al., 2004). However, precise mechanisms for generating these bores were inconclusive from their available data.

Materials and methods

A total of 119 ‘NIOZ4’ self-contained temperature (T) sensors were used sampling at a rate of 1 Hz, with precision better than $0.001 \text{ }^\circ\text{C}$ and a noise level of about $6 \times 10^{-5} \text{ }^\circ\text{C}$. NIOZ4 is an upgrade of NIOZ3 (van Haren et al., 2009), with similar characteristics, except for its reduced size (2/3 smaller). Sensors were taped to a 120 m long nylon-coated 0.0063 m diameter steel cable. They were at 0.6 m vertical intervals in the lower 30 m and at 1.0 m intervals in the upper 90 m of the cable. Originally, 140 sensors were taped to the cable, but during recovery the mooring line unfortunately captured a secondary line that cut-off 21 sensors which were lost. The thermistors were synchronized via induction every 4 h. Thus, timing mismatch was less than 0.02 s. The lowest sensor was 7 m above the bottom and the upper a few m below a single elliptic floatation providing 3000 N of net buoyancy. The float included a downward looking 75 kHz Teledyne-RDI Longranger Acoustic Doppler Current Profiler (ADCP) which sampled erroneously at a relatively slow rate of once per 22.5 min. This taut-wire mooring was deployed at $55^\circ 28.947\text{N}$, $15^\circ 47.852\text{W}$, 919 m water depth and immediately south of a dense CWC-population where the bottom-slope changes sharply (Fig. 1). The high (fisheries) risk of the area and adverse weather conditions did not allow for a longer mooring duration.

The moored observations are supported by extensive shipborne Kongsberg EM302 30 kHz Multibeam observations, for high-resolution bathymetry and genuinely 2D bottom-slope determination, and Seabird 911-plus CTD-profiles. The CTD-data are used to establish a, preferably linear, temperature-density relationship to be able to compute turbulence parameter estimates from the moored thermistor string observations.

The thermistor string data are first converted to conservative temperature (Θ) values (McDougall et al., 2009), before they are used as an estimate for (variations in) potential density anomaly referenced to a level of 1000 dBar (σ_{1000}) following a reasonably tight, constant linear relationship obtained from the CTD data (Fig. 2), $\delta\sigma_{1000} = \alpha\delta\Theta$, $\alpha = -0.13 \pm 0.01 \text{ kg m}^{-3} \text{ }^\circ\text{C}^{-1}$ denoting the thermal expansion coefficient under local conditions (Fig. 2c). The tightness of fit may be called reasonable in the upper temperature range [7.8, 8.7] $^\circ\text{C}$, giving an std = 0.0018 $^\circ\text{C}$ (Fig. 2d). However, it deteriorates in the lower temperature range when cold water moves in, even though the best-fit does not alter much (Fig. 2c and d). This suggests either considerable variation of water masses or, more likely as will be demonstrated in the next section, strong turbulent mixing.

The above ‘tight’ linear temperature–density relationship is the mean for the lower \sim 200 m above the bottom from three CTD-profiles around the main site (the ranges of the ones just before and after the mooring period are shown in Fig. 2). Turbulence parameter estimates are obtained using the moored temperature sensor

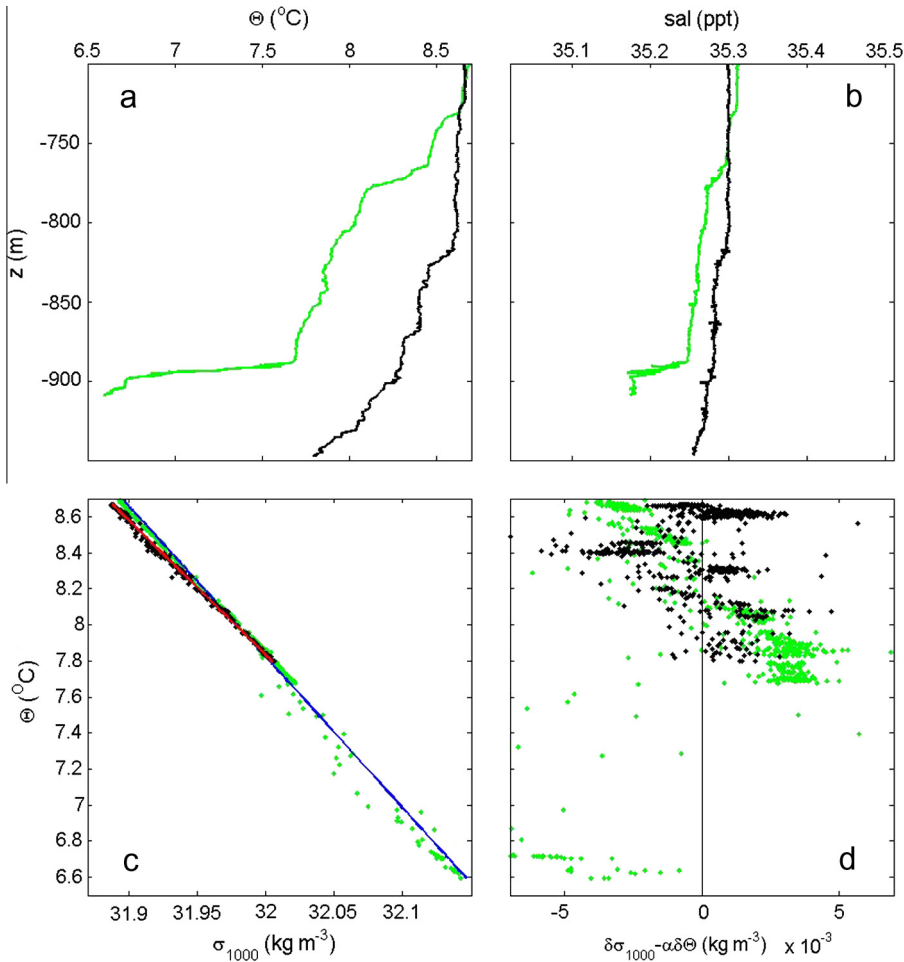


Fig. 2. CTD-observations just prior to deployment (green profiles) and just after recovery (black) of the thermistor string/ADCP mooring, over the lower 200–250 m above the bottom. (a) Conservative temperature. (b) Salinity. (c) Density anomaly (referenced to 1000 m) – conservative temperature relationship, with first order best-fit lines blue and red for green and black data, respectively. (d) Goodness of fit (dotted observations in c – their straight line fits). (For interpretation of the references to color in this figure legend, the reader is referred to the web version of this article.)

data by calculating ‘overturning’ scales. These scales follow after reordering (sorting) every 1 s the 120 m high potential density (conservative temperature) profile, which may contain inversions, into a stable monotonic profile without inversions (Thorpe, 1977). After comparing observed and reordered profiles, displacements (d) are calculated and used for generating the reordered stable profile. Certain tests apply to disregard apparent displacements associated with instrumental noise and post-calibration errors (Galbraith and Kelley, 1996). Such a test-threshold is very low for NIOZ-temperature sensor data, $<5 \times 10^{-4} \text{ }^\circ\text{C}$ (van Haren et al., 2009). The turbulence dissipation rate is then,

$$\varepsilon = 0.64d^2N^3, \quad (3)$$

where $N = (-g/\rho_0\delta\sigma_{1000}/\delta z)^{1/2}$ denotes the buoyancy frequency computed from each of the reordered, essentially statically stable, vertical density profiles (and g denotes acceleration of gravity and $\rho_0 = 1026 \text{ kg m}^{-3}$ a constant reference density). The numerical constant follows from empirically relating the overturning scale with the Ozmidov-scale $L_O = 0.8d$ (Dillon, 1982). Estimating vertical turbulent diffusivity $K_z = \Gamma\varepsilon N^{-2}$ wherein a constant mixing efficiency $\Gamma = 0.2$ is used (Osborn, 1980; Oakey, 1982; Klymak et al., 2008) for conversion of kinetic into potential energy, we find,

$$K_z = 0.128d^2N. \quad (4)$$

In Eqs. (3) and (4) we use individual values of d to replace overturning scales, rather than taking their rms-value across a single

overturn as originally proposed by Thorpe (1977). The reason is that we cannot easily distinguish individual overturns, first, because overturns are found at various scales with small ones overwriting larger overturns, precisely as one expects from turbulence, and, second, because some exceed the range of temperature sensors. Instead, we first calculate non-averaged values of d in Eqs. (3) and (4) for high-resolution images of $K_z(z, t)$ and $\varepsilon(z, t)$. Subsequently, we calculate ‘mean’ turbulence parameter values by averaging the parameters in the vertical [] or in time $\langle \rangle$, or both.

The errors in the mean turbulence parameter estimates thus obtained depend on the error in N , i.e., the error in the temperature–density relationship, while the instrumental noise error of the thermistors is negligible. Given the errors, the estimated uncertainty in time–depth mean estimates of Eqs. (3) and (4) amounts about a factor of 2. Using similar temperature sensor data from Great Meteor Seamount, van Haren and Gostiaux (2012) found mean turbulence parameter estimate values to within a factor of 2 similar to those inferred from ship-borne CTD/LADCP profiler data near the bottom. Their values complied well with profiler-based estimates in similar sloping bottom areas by Klymak et al. (2008).

Observations

The Multibeam bathymetry (Fig. 1b–d) based local bottom slope was $\gamma \approx 0.2$ (10°), close to the foot of the steep southeastern

slope of a CWC-mound. Using local CTD observations (Fig. 2) to determine a ‘mean’ large-scale buoyancy frequency $N = 3 \pm 1 \times 10^{-3} \text{ s}^{-1}$ (computed using three profiles obtained at different times in the area and using a vertical scale of 200 m directly above the bottom), we compare this slope with the freely propagating internal wave slope in Eq. (2) and that of sub-inertial bottom-trapping in Eq. (1b).

On the horizontal scale O(100) km of the entire Rockall Bank (Fig. 1a), and using a 1×1 km interpolation scheme of GEBCO bottom-topography data, relatively small bottom slopes are generally found on the Bank and in the deep trough to its east, with steepest slopes $>2.5^\circ$ for water depths [1000 m (red-yellow)–3500 m (dark-blue)]. According to Eqs. (1) and (2), the red contour of both diurnal near-bottom wave trapping and semidiurnal critical reflection is computed around the 1000 m water depth on the east and southeast slopes of Rockall Bank. The condition for sub-inertial double trapping is indicated by the black contour. Thus, diurnal (sub-inertial) baroclinic wave trapping between the red and black lines is predicted in very narrow depth ranges (barely visible in parts of Fig. 1a), on the shallow side close to the 1000 m contour (yellow-orange). Only on the southeast slopes, around 55.5°N , 16°W where the Logachev CWC-mound area is situated, the contours become rugged and the depth range relatively broad. Recall that the coarse grid ($\sim 30 \times 30$ km) numerical model by Pingree and Griffiths (1984) predicts barotropic wave trapping with enhanced diurnal currents across a considerable part of the Bank for water depths <1000 m.

In the Logachev CWC-mound detail on a smoothed 250×250 m grid (Fig. 1b) from 15×30 m Multibeam data (Fig. 1c and d), the black and red slope-contours reverse position with respect to the mound’s summit. Again, a narrow band is observed between the red and black contours, on the south-side around the 1000 m water depth contour. Variations in 100-m-vertical-scale-computed N barely make a difference, as dashed contours ($N \pm 1$ std) are close to the solid ones (mean N). The mooring location is seen at a slightly steeper slope summit-ward of the water-depth-range where semidiurnal critical reflection and sub-inertial (diurnal) bottom trapping are expected. However, the distance to the black contour of the ‘inertial-slope-criterion’ in Eq. (1b) is less than a kilometer (~ 700 m), which is comparable to the semidiurnal tidal excursion length of 600 m and well less than the diurnal excursion length of 3300 m.

Hydrographically, the CTD-data from stations less than 1 km from the mooring show that temperature dominates over salinity in terms of density variations over most of the lower half of the local water column (Fig. 2a and b; the range of the two scales compensate in density). Vertical density stratification varies considerably, depending on the time of observations. Relatively warmer (and saltier) waters are alternated with relatively cooler (slightly fresher) waters, with largest variations closest to the bottom. Such variations at different depths somewhat hamper the construction of the ‘tight’, linear temperature–density relationship.

Entire time series

With reference to the ADCP’s pressure (p) sensor, the taut-wire mooring did not move more than about ± 0.1 m vertically due to mooring drag. This was anticipated given the current magnitudes $<0.3 \text{ m s}^{-1}$ and the large buoyancy elements used. The observed pressure variations are mainly due to surface elevations, which are dominated by a barotropic semidiurnal tide. Over the 9 days of observations this tide varies from barely 1 m vertical variation, just before neaps, to more than 3 m variation, just after springs (Fig. 3b). In contrast, the deep sea interior is dominated by motions that have a diurnal (baroclinic tidal) character with much larger vertical amplitudes (Fig. 3 and 4).

This rather unusual dominance of baroclinic diurnal tide is reflected, except in pressure, in all observed variables, including temperature, horizontal and vertical current components and acoustic echo amplitude. Over the 120 m vertical range of observations, starting 7 m above the bottom (mab), these tidal variations are quite uniform. Harmonic analysis of the K_1 (dominant diurnal tidal component, which is indistinguishable from O_1 and solar S_1 for the 9-days record) shows a current amplitude decrease from 0.12 to $0.095 (\pm 0.005) \text{ m s}^{-1}$ between $z = -900$ and -820 m. This suggests bottom-enhanced or bottom-trapped currents. Between $z = -900$ and -870 m the phase of this diurnal tidal current is uniform, to within the $\pm 5^\circ$ uncertainty, but it changes monotonically by 20° between -870 and -820 m. In contrast, the weaker semidiurnal (M_2) tidal current varies from 0.03 to $0.05 (\pm 0.005) \text{ m s}^{-1}$ between -900 and -820 m, with a similar phase variation as the diurnal current. These observations suggest a baroclinic tide having one wavelength over the 900 m vertical range, for both constituents.

The baroclinic (diurnal) tide vertical amplitude of variations is not resolved by the mooring, implying large (>125 m high) waves. With time, the modulation of amplitude is different between the variables, none of which follow the semidiurnal spring-neap cycle of the surface tide. The modulation of along-slope diurnal current variations (Fig. 3c) approaches that of the barotropic (pressure) tide variations most; it also intensifies towards the end of the record. However, cross-slope (Fig. 3d) and vertical (Fig. 3e) current components have largest amplitudes in the first few days of the record, while echo amplitude (Fig. 3b) is largest in the middle part of the record.

A correlation between temperature (Fig. 3a) and echo amplitude variations is not found significant to the 95% level, but highest values of echo are regularly observed at the turn from up- to down-slope (cooling to warming) phase of the tide, especially in the upper half of the record (between about -870 and -820 m). A lesser, secondary echo-amplitude-maximum per diurnal period is observed during the beginning of the upslope cooling phase. As a result, echo amplitude is more or less inversely related with temperature. This contrasts with optical backscatter and fluorescence observations by Duineveld et al. (2007) obtained at about 1 m from the bottom on a site 30 km westward of the present location. Those observations were strictly in phase with temperature for fluorescence and more or less in phase with temperature, except for a backscatter increase at the turn from warming to cooling phase. It is noted that the mounds at that observational site were smaller and more or less oriented across-slope, compared to the mound in the present area. Although acoustic backscatter is differently sensitive than optical backscatter, we assume that both more or less indicate similar variations of suspended particles. For a 75 kHz ADCP, acoustic reflection (echo amplitude) is most sensitive to particles and zooplankton having sizes of 0.008–0.01 m. For the present data, it has not been verified by towing nets which particles dominate the acoustic reflection. The echo amplitudes thus provide qualitative data only.

Like in the echo amplitude, the diurnal tide is also less dominant in the vertically averaged turbulence dissipation rate (Figs. 3f, and 4-green¹ spectrum). Largest spectral levels are found, insignificantly peaking, in the diurnal(O_1 , K_1), semidiurnal(M_2)/inertial(f) and terdiurnal(M_3) frequency bands. The latter is probably due to interaction between diurnal and semi-diurnal motions. The turbulence dissipation rate spectrum best resembles the shear spectrum (Fig. 4-blue). At frequencies higher than inertial, both spectra fall off in power with a slope of -1 . This suggests shear-driven

¹ For interpretation of color in Figs. 3–5 and A1, the reader is referred to the web version of this article.

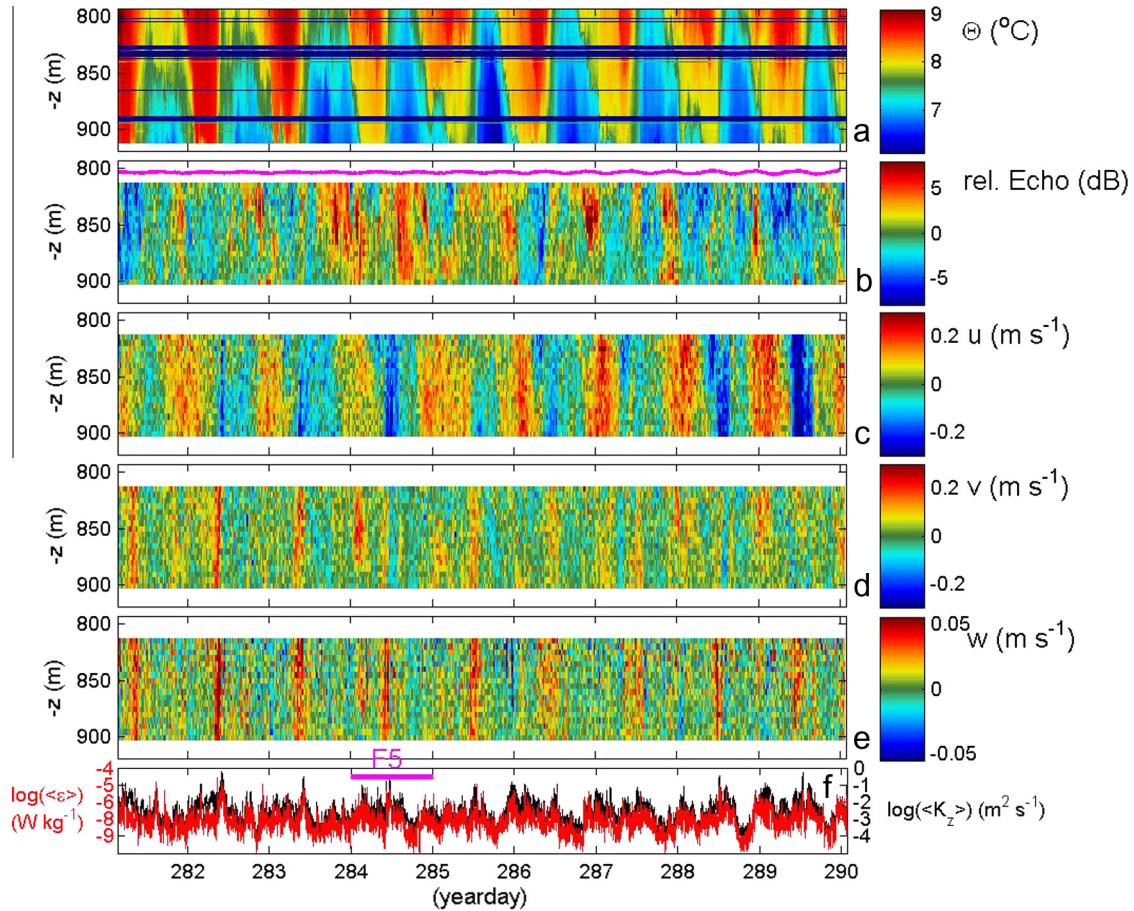


Fig. 3. Overview of entire moored near-bottom thermistor string/ADCP observations. (a) Depth-time series of conservative temperature from 119 1-Hz sampling sensors between [7, 126] mab (m above the bottom). Data from a further 21 sensors are missing (horizontal lines). (b) Depth-time series of acoustic echo amplitude relative to the time mean at each depth level. Below 905 m data are unreliable due to direct bottom reflection of first main sidelobe. Purple graph indicates pressure variations (in dB ~ m) around their mean of 804 m. (c) Depth-time series of East–West, ~along-isobath current component. (d) Corresponding North–South, ~cross-slope component. (e) Corresponding vertical current component. (f) Time series of vertically averaged dissipation rate (red) and eddy diffusivity (black) estimated using (interpolated) thermistor string data in (a) following the method described in the Materials and Methods Section. The purple bar (F5) indicates the period of Fig. 5. (For interpretation of the references to colour in this figure legend, the reader is referred to the web version of this article.)

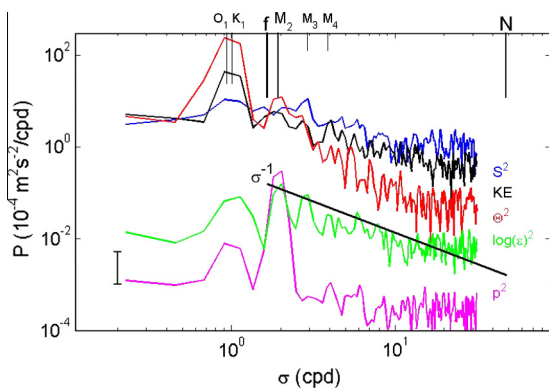


Fig. 4. Weakly smoothed spectra for data (sub)sampled at the rate of the ADCP. Shown are kinetic energy (black) at 860 m, shear-squared $|S|^2$ over 820–900 m (blue; arbitrary scale in s^{-2}/cpd), pressure variance p^2 at 792 m (purple; arbitrary scale in $(N m^{-2})^2/cpd$), conservative temperature variance θ^2 (red; arbitrary scale in $^{\circ}C^2/cpd$) at 860 m and $\log \langle \epsilon \rangle^2$ (green, arbitrary scale in $W^2 kg^{-2}/cpd$) averaged over the range 793–912 m. On the top, several tidal constituent are indicated (diurnal O_1 and K_1 , semidiurnal lunar M_2 , ter-diurnal M_3 and quarter-diurnal M_4). Also, the local inertial frequency f is indicated. (For interpretation of the references to colour in this figure legend, the reader is referred to the web version of this article.)

turbulence dominates over convective turbulent overturning, while it is predominantly generated and varies at tidal/inertial frequencies, or the lower internal wave frequencies, as expected. The turbulence parameter values averaged over the entire mooring period of 9 days and over the range of sensors between 7 and 126 mab amount $\langle \{\epsilon\} \rangle = 2.2 \pm 1.1 \times 10^{-7} v W kg^{-1}$ and $\langle \{K_z\} \rangle = 9 \pm 5 \times 10^{-3} m^2 s^{-1}$, while $\langle [N] \rangle = 3.2 \pm 1 \times 10^{-3} s^{-1}$.

One day zoom

A zoom of one day of data shows an asymmetry of the internal tide above sloping topography, in this case with diurnal periodicity (Fig. 5). If one follows the light-blue color-transition to dark-blue, the warming, downslope moving phase takes longer in time than the cooling, upslope phase (Fig. 5a). Stratification organizes in thin layers throughout the day (Fig. 5b). These thin layers are pushed towards the bottom during the warming phase (note that the lowest sensor was about 7 mab). Prior to and after the rapid ‘frontal’ change to upslope phase, relatively large homogeneous layers are formed which contain >50 m large overturns (Fig. 5c). In such near-homogeneous layers mixing-efficiency may not be high because of the weak stratification, but throughout the upslope phase thin layers are observed and which contain relatively high dissipation rates. The period of minimum dissipation rates (over

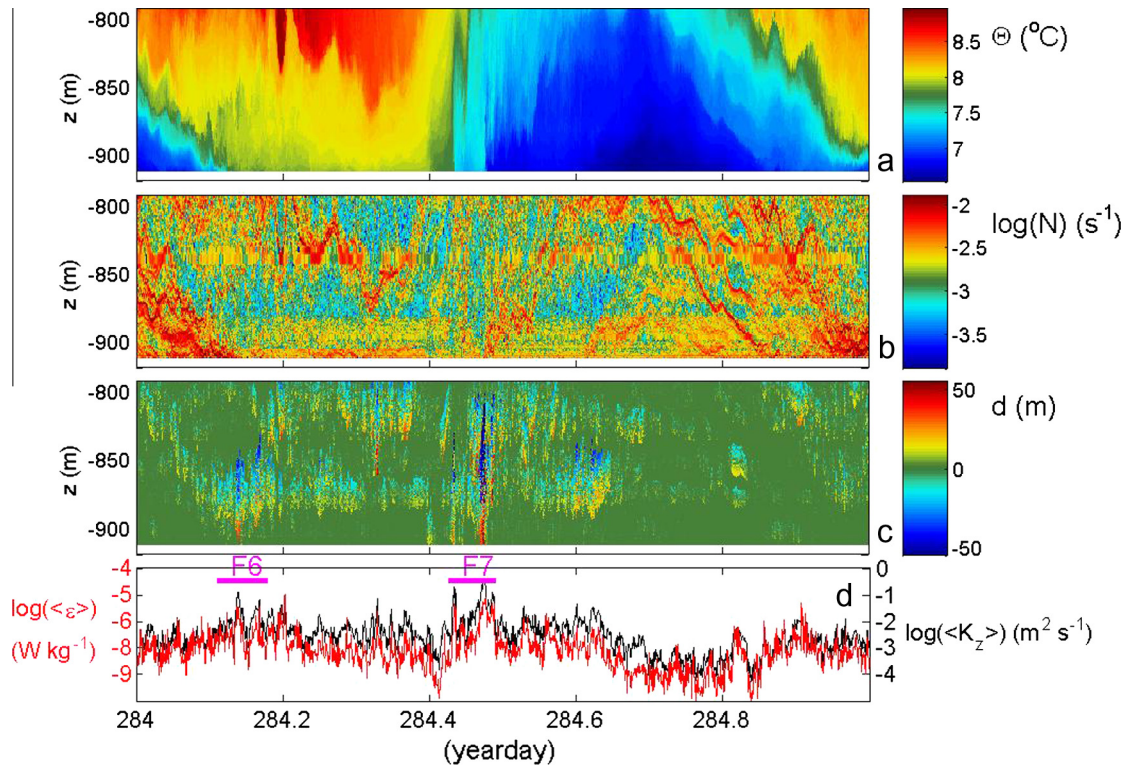


Fig. 5. One day, \sim one diurnal tidal period example of high-resolution thermistor string observations. (a) Depth-time series of conservative temperature, missing sensors interpolated. (b) Depth-time series of buoyancy frequency computed from a. after reordering to stable vertical profiles, every time step. The horizontal lines reflect the interpolated missing sensors. (c) Depth-time series of displacements between observed and reordered temperature profiles. (d) Time series of dissipation rate (red) and eddy diffusivity (black) using data in a. Periods of Figs. 6 and 7 are indicated by purple bars. (For interpretation of the references to colour in this figure legend, the reader is referred to the web version of this article.)

the range of observations) is found around the start of the warming phase (Fig. 5d). In this period, dips in turbulence parameter estimates are about four orders of magnitude lower than peaks in the one day record. For this one day of observations, the average turbulence parameter values are $\langle [\varepsilon] \rangle = 2.5 \pm 1.6 \times 10^{-7} \text{ W kg}^{-1}$ and $\langle [K_z] \rangle = 8 \pm 4 \times 10^{-3} \text{ m}^2 \text{ s}^{-1}$, while $\langle [N] \rangle = 3.1 \pm 1 \times 10^{-3} \text{ s}^{-1}$.

Warming tidal phase detail

A 1.7 h zoom of the warming downslope moving tidal phase demonstrates that what occurred as spikes in the dissipation rates (Fig. 5d) are in fact $\sim 1000 \text{ s}$ periods of intense mixing (Fig. 6d). During this tidal phase, none of this mixing reaches the bottom. These periods are associated with asymmetric nonlinear wave formation in thin layers that overturn in surrounding weaker stratified layers, e.g., on day 284.135. For the entire 1.7 h period, we computed average values of $\langle [\varepsilon] \rangle = 5 \pm 3 \times 10^{-7} \text{ W kg}^{-1}$, $\langle [K_z] \rangle = 1.6 \pm 0.8 \times 10^{-2} \text{ m}^2 \text{ s}^{-1}$. These values are double that of tidal-period mean values. This indicated that during the relatively slow warming phase, waters can occasionally also be quite intensely turbulent, although at distances of 10–50 mab. The mean $\langle [N] \rangle = 2.7 \pm 1 \times 10^{-3} \text{ s}^{-1}$, so that the buoyancy period is about 2300 s (purple bar in Fig. 5d). As a result, the observed overturns thus have shorter duration than the shortest possible free internal wave period. However, the two largest clusters of overturns (between days 284.132 and 284.146, and between 284.154 and 284.168), do approach the buoyancy period scale.

Transition to cooling tidal phase detail

Even more intense turbulence is observed during the transition between warming down- and cooling upslope phases (Fig. 7). This

is similar to observations in areas where freely propagating semi-diurnal internal tide (van Haren and Gostiaux, 2012) and sub-inertial-driven upslope moving bores (Hosegood et al., 2004) dominate sediment resuspension. For the 1.6 h period depicted here, average turbulence parameters are $\langle [\varepsilon] \rangle = 1.2 \pm 0.6 \times 10^{-6} \text{ W kg}^{-1}$, $\langle [K_z] \rangle = 5 \pm 3 \times 10^{-2} \text{ m}^2 \text{ s}^{-1}$, $\langle [N] \rangle = 2.4 \pm 1 \times 10^{-3} \text{ s}^{-1}$. In the presented case, a double front (two fronts $\sim 1 \text{ h}$ apart) is observed, with almost 100 m high overturns. Although our ADCP sampling resolution was quite coarse, the fronts-associated vertical currents exceed 0.05 m s^{-1} (Fig. 3e).

Turbulence parameter estimates using CTD data

The depth-time averaged turbulence estimates using thermistor string data may be compared with estimates using corrected density anomaly data from three CTD-profiles obtained just before and just after the time-series-period in the vicinity of the mooring. Averaged over the lower half (–950, –500) m of the CTD-profiles we find $\langle [\varepsilon] \rangle = 2.8 \pm 1.4 \times 10^{-7} \text{ W kg}^{-1}$, $\langle [K_z] \rangle = 1.2 \pm 0.5 \times 10^{-2} \text{ m}^2 \text{ s}^{-1}$, $\langle [N] \rangle = 2.5 \pm 1 \times 10^{-3} \text{ s}^{-1}$. These values compare very well to within one standard deviation with the vertically averaged estimates using temperature sensor data in the One day zoom Section, when an averaging period of about a day or longer is considered. The slightly (15–30%) lower turbulence parameter values for the thermistor string data may be due to (low-)bias following the linear interpolation of the 21 missing sensors, so that small-scale overturns cannot be computed. The goodness of comparison is found despite the rather poor temporal resolution but better vertical resolution of the CTD-data compared with the thermistor string data. It confirms the tightness of the temperature-density relationship, so that turbulence parameter estimates are reliably estimated using moored thermistor string data. It also shows that just a few

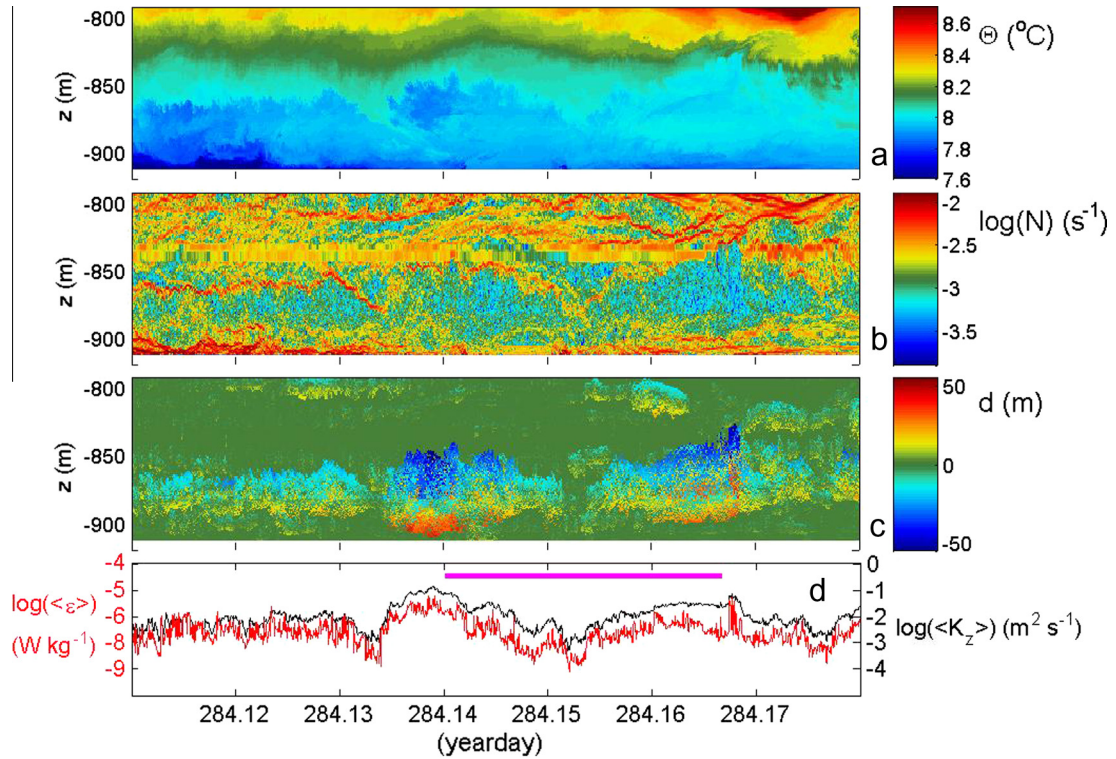


Fig. 6. As Fig. 5, but for a 1.7 h detail during the warming, downslope phase. Note the different scale in a. The mean buoyancy period (~ 2300 s) is indicated by the purple bar in d.

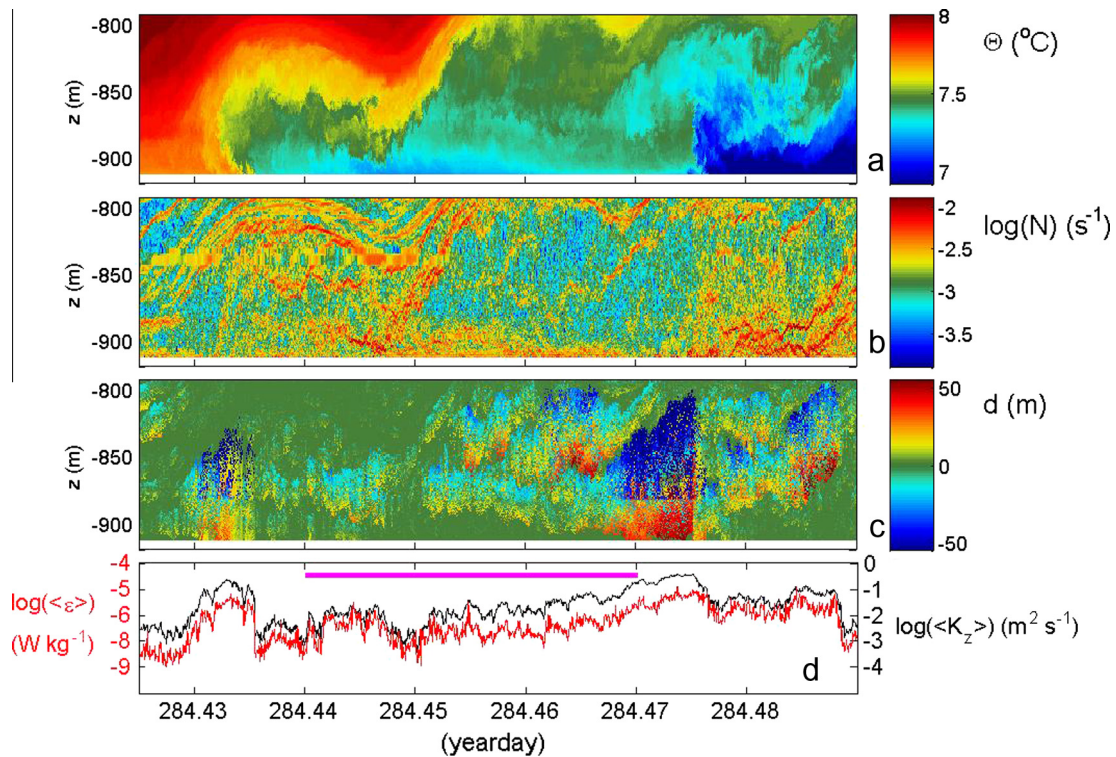


Fig. 7. As Fig. 5, but for a 1.6 h detail mainly during the cooling, upslope phase. Note the different scale in a. The mean buoyancy period (~ 2600 s) is indicated by the purple bar in d.

CTD-(or microstructure) profiler data over a suitable vertical range (here, 500 m) are needed for a statistical convergence. Naturally, sampling through high-turbulence periods like in Fig. 7 are a matter of ‘luck’, given that these occur less than 5% of time.

Discussion and conclusions

The present estimated turbulence dissipation rates are comparable, to within one standard deviation or less than a factor of

two, with recent estimates of breaking internal waves above various deep-sea sloping topography where free propagating semi-diurnal internal tides dominate (van Haren and Gostiaux, 2012; van Haren and Greinert, 2013). The value of $[\langle \varepsilon \rangle] = (2 \pm 1) \times 10^{-7} \text{ W kg}^{-1}$ found in these areas is also comparable with those observed just seaward of the shelf-break where very energetic tides are found on the relatively shallow Malin Shelf (Inall et al., 2000) and in the Celtic Sea (recent observations presented in 2013: <http://folk.uio.no/johng/waves13/summaries/AleynikInall.pdf>). This implies that internal wave dissipation above deep-sea topography can be as intense as shallow sea internal tide dissipation rates. Internal wave dissipation is thus not exclusively found in the strongly stratified layers near the ocean surface.

As previously observed for freely propagating semidiurnal internal tides (van Haren and Gostiaux, 2012), the fronts observed here for trapped diurnal waves are the only (two) overturns that extend from the bottom upwards per tidal period. Thereby, these short passages potentially directly influence sediment (resuspension and redeposition) and benthic life (nutrient/food supply). These processes are likely extremely important for CWC, increasing the food and particle supply and flushing of the coral framework, but also making nutrients several times available to the corals and associated species. Noting that none of the frontal bores associated with freely propagating semidiurnal tides have been found above critical slopes so far (see also van Haren and Greinert, 2013), it seems that nonlinear bore development is associated with a different process. This is further evidenced here, where the bores cannot be associated with critical reflection as this process does not exist at the diurnal frequency. This is because diurnal baroclinic waves are not freely propagating waves. However, the diurnal waves are trapped and driven to near-resonance, and thus strongly amplified near the bottom. Their particular depth/buoyancy frequency range is half a major axis (or full minor axis) excursion length from where most densely populated CWC are found (see Appendix for tidal ellipses).

Although more additional (including modeling) work is needed to precisely establish: (1) why especially the K_1 -diurnal tide is driven to resonance, (2) why CWC are most dense above steepest slopes, and (3) how the transfer of energy occurs from linear large-scale baroclinic waves to non-linear breaking waves, e.g. via a hydraulic jump over the mound, it seems likely that all are associated with baroclinic bottom-trapped waves here. The expected phase speed of $\sim 0.15 \text{ m s}^{-1}$ for resonant diurnal baroclinic motions around a CWC-mound is close to the observed near-bottom diurnal tidal particle velocity of 0.12 m s^{-1} . We note that this speed is considerably smaller than CWC-associated current speeds reported previously. We conclude that turbulence generation, here via internal wave breaking, is a more important parameter for CWC-growth than current speed.

Given the relatively small observed vertical phase change, the baroclinic tidal motions have a vertical scale of about the local water depth, with a near-bottom enhancement of amplitude, presumably due to resonance around the CWC. Thus a relationship is observed between the size of the mound and the current amplification. It is noted that the major axis of the diurnal current ellipse direction (see Appendix) is more or less in the direction of the CWC, which is closely aligned with the isobaths. As explained in the Appendix, this mean alignment of orientations does not favor a shaping of the CWC-mound by the associated average (residual) currents, but individual (modulated) diurnal tidal currents can do so. Thus, baroclinic tidal motions may maintain a CWC-mound, like barotropic tidal currents maintain sandbanks in shallow seas (Appendix). Further relationship is expected by the more than 120 m high internal waves pumping water up- and down along- and across the sloping bottom, thereby potentially replenishing

nutrients. The horizontal diurnal particle displacements of $\sim 3 \text{ km}$ cover the entire mound, when oriented at an angle away from the major mound axis. Thereby, the upslope proceeding bores over the bottom seem important in terms of turbulence and particle motion, as previously observed for sediment resuspension in the Faeroe-Shetland Channel. However, in the present region also the transition from upslope to downslope movement also carries substantial turbulence some distance off the bottom. It may thus provide nutrients from higher-up, as was found previously, but differently linked strictly to warmer water, on an adjacent mound in the Logachev area (Duineveld et al. 2007). The high waves and excursion length observed here thus also may determine the growth-height of CWC-mounds, which seem to be limited to about 600 m (Fig. 1d), or a particular temperature level of roughly 9°C .

Acknowledgments

We thank captain and crew of the R/V Pelagia. We thank M. Laan for his ceaseless thermistor efforts, H. de Haas and N. Krijgsman for producing Fig. 1 and L. Maas for tidal advice. This work has been financed in part by the Netherlands Organization for Scientific Research (NWO).

Appendix. Tidal current ellipses and mound orientation

White et al. (2007) suggested that for some CWC-mound sites around Rockall Through, including Rockall and Porcupine Banks, mound clusters were shaped in the direction of the major axis of the dominant tidal currents across the major isobaths. In the present Logachev mound area, the dominant diurnal tidal current ellipse (Fig. A1) is observed to be closely elongated along the major axis of the mound which is aligned with the isobaths of the Rockall Bank. Although we identify only one mound here (cf. Fig. 1) and not the orientation of a cluster, this observation complies with the findings of White et al. (2007), except that the current ellipse and mound orientation are along the major isobaths, instead of across. Also, the almost negligible angle between mean current ellipse and mound orientation does not comply with the 2D-theory of sandbank maintenance by residual currents generated through barotropic tidal currents in shallow seas and for which an optimum angle of $10\text{--}15^\circ$ ($>5^\circ$) is required between the two orientations (Zimmerman, 1981, 1986; Sanay et al., 2007). We identify two explanations for these discrepancies between observations and theory.

First, the mean baroclinic tidal ellipse (blue in Fig. A1) may be oriented along the major axis of the mound (red line in Fig. A1), but the intermittent, modulated individual current ellipses show a large variety of angles, between $[0\ 45^\circ]$. This is evidenced from diurnal band-pass filtered data (purple in Fig. A1).

Second, the weaker mean semidiurnal tidal current ellipse (green in Fig. A1) is oriented at an angle of about 70° with the mound orientation. However, given the average $|\mathbf{U}_{M2}| = 0.04 \text{ m s}^{-1}$ current amplitude, the associated excursion length of $2|\mathbf{U}_{M2}|/\sigma \approx 600 \text{ m}$ is too small compared with the $\sim 4000 \text{ m}$ length scale of the mound. For resonant residual circulation and mound maintenance (or growth), these two length scales should be approximately equal and the orientation of the mound should be directed anticlockwise from the direction of major tidal current ellipse-axis (Zimmerman, 1981). As this is nearly the case for the 0.12 m s^{-1} diurnal current amplitude ($2|\mathbf{U}_{K1}|/\sigma \approx 3300 \text{ m}$), and for a number of individual diurnal current ellipses (Fig. A1, purple), it is concluded that the (modulated) intermittent resonant bottom-trapped baroclinic diurnal tidal ellipse currents can shape the mound.

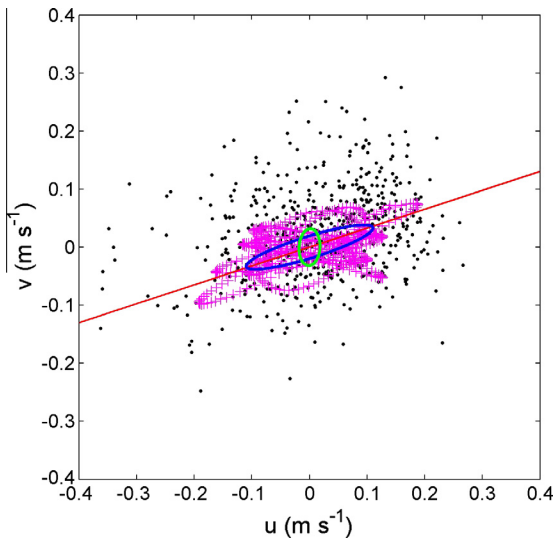


Fig. A1. Current data observed at 870 m and compared to CWC-mound orientation (red line). Raw data are given in black dots, diurnal band-pass filtered data in purple crosses. The 9-day mean harmonic diurnal current ellipse is shown in blue, while the semidiurnal one in green. (For interpretation of the references to color in this figure legend, the reader is referred to the web version of this article.)

References

- Cacchione, D., Wunsch, C., 1974. Experimental study of internal waves over a slope. *Journal of Fluid Mechanics* 66, 223–239.
- Cacchione, D.A., Drake, D.E., 1986. Nepheloid layers and internal waves over continental shelves and slopes. *Geo-Marine Letters* 6, 147–152.
- Cartwright, D.E., 1969. Extraordinary tidal currents near St Kilda. *Nature* 223, 928–932.
- Crawford, W.R., Thomson, R.E., 1982. Continental shelf waves of diurnal period along Vancouver Island. *Journal of Geophysical Research* 87, 9516–9522.
- Davies, A.J., Duineveld, G.C.A., Lavaleye, M.S.S., Bergman, M.J.N., van Haren, H., Roberts, J.M., 2009. Downwelling and deep-water bottom currents as food supply mechanisms to the cold-water coral *Lophelia pertusa* (Scleractinia) at the Mingulay Reef complex. *Limnology and Oceanography* 54, 620–629.
- De Mol, B., Van Rensbergen, P., Pillen, S., Van Herreweghe, K., Van Rooij, D., McDonnell, A., Huvenne, V., Ivanov, M., Swennen, R., Henriët, J.P., 2002. Large deep-water coral banks in the Porcupine Basin, southwest of Ireland. *Marine Geology* 188, 193–231.
- Dickson, R.R., McCave, I.N., 1986. Nepheloid layers on the continental slope west of Porcupine Bank. *Deep-Sea Research* 33, 791–818.
- Dillon, T.M., 1982. Vertical overturns: a comparison of Thorpe and Ozmidov length scales. *Journal of Geophysical Research* 87, 9601–9613.
- Dorschel, B., Hebbeln, D., Foubert, A., White, M., Wheeler, A.J., 2007. Hydrodynamics and cold-water coral facies distribution related to recent sedimentary processes at Galway Mound west of Ireland. *Marine Geology* 244, 184–195.
- Duineveld, G.C.A., Lavaleye, M.S.S., Bergman, M.J.N., de Stigter, H., Mienis, F., 2007. Trophic structure of a cold-water coral mound community (Rockall Bank, NE Atlantic) in relation to the near-bottom particle supply and current regime. *Bulletin of Marine Science* 81, 449–467.
- Foldvik, A., Middleton, J.H., Foster, T.D., 1990. The tides of the southern Weddell Sea. *Deep-Sea Research* 37, 1345–1362.
- Frederiksen, R., Jenssen, A., Westerberg, H., 1992. The distribution of the scleractinian coral *Lophelia pertusa* around the Faeroe Islands and the relation to internal tidal mixing. *Sarsia* 77, 157–171.
- Freiwald, A., 2003. Reef-forming cold-water corals. In: Wefer, G., Billett, D., Hebbeln, D., Jørgensen, B.B., Schlüter, M., van Weering, T.C.E. (Eds.), *Ocean Margin Systems*. Springer-Verlag, Berlin, pp. 365–385.
- Galbraith, P.S., Kelley, D.E., 1996. Identifying overturns in CTD profiles. *Journal of Atmospheric and Oceanic Technology* 13, 688–702.
- Henry, L.-A., Roberts, J.M., 2007. Biodiversity and ecological composition of macrobenthos on cold-water coral mounds and adjacent off-mound habitat in the bathyal Porcupine Seabight, NE Atlantic. *Deep Sea Research Part I* 54, 654–672.
- Hosegood, P., Bonnin, J., van Haren, H., 2004. Solibore-induced sediment resuspension in the Faeroe-Shetland Channel. *Geophysical Research Letters* 31, L09301. <http://dx.doi.org/10.1029/2004GL019544>.
- Huthnance, J.M., 1974. On the diurnal tidal currents over the Rockall Bank. *Deep-Sea Research* 21, 23–35.
- Inall, M.E., Rippeth, T.P., Sherwin, T.J., 2000. Impact of nonlinear waves on the dissipation of internal tidal energy at a shelf break. *Journal of Geophysical Research* 105, 8687–8705.
- Kenyon, N.H., Akhmetzhanov, A.M., Wheeler, A.J., van Weering, T.C.E., de Haas, H., Ivanov, M.K., 2003. Giant carbonate mud mounds in the southern Rockall Trough. *Marine Geology* 195, 5–30.
- Klymak, J.M., Pinkel, R., Rainville, L., 2008. Direct breaking of the internal tide near topography: Kaena Ridge, Hawaii. *Journal of Physical Oceanography* 38, 380–399.
- Lam, F.-P.A., 1999. Shelf waves with diurnal tidal frequency at the Greenland shelf edge. *Deep Sea Research Part I* 46, 895–923.
- Lindberg, B., Berndt, C., Mienert, J., 2007. The Fugløy Reef at 70°N: acoustic signature, geologic, geomorphologic and oceanographic setting. *International Journal of Earth Sciences* 96, 201–213.
- Longuet-Higgins, M.S., 1968. On the trapping of waves along a discontinuity of depth in a rotating ocean. *Journal of Fluid Mechanics* 31, 417–434.
- McDougall, T.J., Feistel, R., Millero, F.J., Jackett, D.R., Wright, D.G., King, B.A., Marion, G.M., Chen, C.-T.A., Spitzer, P., 2009. Calculation of the thermodynamic properties of seawater. *Global Ship-based Repeat Hydrography Manual*, IOCCP Report 14, ICPO Publication Series 134, U.N.E.S.C.O., Paris (F), 131 pp.
- Mienis, F., van Weering, T., de Haas, H., de Stigter, H., Huvenne, V., Wheeler, A., 2006. Carbonate mound development at the SW Rockall Trough margin based on high resolution TOBI and seismic recording. *Marine Geology* 233, 1–19.
- Mienis, F., de Stigter, H.C., White, M., Duineveld, G., de Haas, H., van Weering, T.C.E., 2007. Hydrodynamic controls on cold-water coral growth and carbonate-mound development at the SW and SE Rockall Trough Margin, NE Atlantic Ocean. *Deep Sea Research Part I* 54, 1655–1674.
- Mienis, F., de Stigter, H.C., de Haas, H., van Weering, T.C.E., 2009. Near-bed particle deposition and resuspension in a cold-water coral mound area at the Southwest Rockall Trough margin, NE Atlantic. *Deep Sea Research Part I* 56, 1026–1038.
- Moray, R., 1665. A relation of some extraordinary tydes in the West-isles of Scotland. *Philosophical Transactions of the Royal Society of London* 1, 53–55.
- Oakey, N.S., 1982. Determination of the rate of dissipation of turbulent energy from simultaneous temperature and velocity shear microstructure measurements. *Journal of Physical Oceanography* 12, 256–271.
- Osborn, T.R., 1980. Estimates of the local rate of vertical diffusion from dissipation measurements. *Journal of Physical Oceanography* 10, 83–89.
- Pingree, R.D., Griffiths, D.K., 1984. Trapped diurnal waves on Porcupine and Rockall Banks. *Journal of the Marine Biological Association of the United Kingdom* 64, 889–897.
- Rhines, P.B., 1970. Edge-, bottom-, and Rossby waves. *Geophysical and Astrophysical Fluid Dynamics* 1, 273–302.
- Rhines, P.B., 1977. The dynamics of unsteady currents. In: Goldberg, E.D., McCave, I.N., O'Brien, J.J., Steele, J.H. (Eds.), *The Sea*, vol. 6. Wiley-Interscience, New York, USA, pp. 89–318.
- Sanay, R., Vougaris, G., Warner, J.C., 2007. Tidal asymmetry and residual circulation over linear sandbanks and their implication on sediment transport: a process-oriented numerical study. *Journal of Geophysical Research* 112, C12015. <http://dx.doi.org/10.1029/2007JC004101>.
- Thorpe, S.A., 1977. Turbulence and mixing in a Scottish loch. *Philosophical Transactions of the Royal Society of London A* 286, 125–181.
- Thorpe, S.A., Keen, J.M., Jiang, R., Lemmin, U., 1996. High frequency internal waves in Lake Geneva. *Philosophical Transactions of the Royal Society of London A* 354, 237–257.
- van Haren, H., Gostiaux, L., 2012. Detailed internal wave mixing above a deep-ocean slope. *Journal of Marine Research* 70, 173–197.
- van Haren, H., Greinert, J., 2013. Variability of internal frontal bore breaking above Opouawe Bank methane seep area (New Zealand). *Geochemistry, Geophysics, Geosystems* 14, 2460–2473. <http://dx.doi.org/10.1002/ggge.20170>.
- van Haren, H., Laan, M., Buijsman, D.-J., Gostiaux, L., Smit, M.G., Keijzer, E., 2009. NIOZ3: independent temperature sensors sampling yearlong data at a rate of 1 Hz. *IEEE Journal of Oceanic Engineering* 34, 315–322.
- van Oevelen, D., Duineveld, G., Lavaleye, M., Mienis, F., Soetaert, K., Heip, C.H.R., 2009. The cold-water coral community as a hot spot for carbon cycling on continental margins: a food-web analysis from Rockall Bank (northeast Atlantic). *Limnology and Oceanography* 54, 1829–1844.
- van Raaphorst, W., Malschaert, H., van Haren, H., Boer, W., Brummer, G.-J., 2001. Across-slope zonation of erosion and deposition in the Faeroe-Shetland Channel, North Atlantic Ocean. *Deep Sea Research Part I* 48, 567–591.
- van Weering, T.C.E., de Haas, H., de Stigter, H.C., Lykke-Andersen, H., Kouvaev, I., 2003. Structure and development of giant carbonate mounds at the SW and SE Rockall Trough margins, NE Atlantic Ocean. *Marine Geology* 198, 67–81.
- Wheeler, A.J., Beyer, A., Freiwald, A., de Haas, H., Huvenne, V.A.I., Kozachenko, M., Olu-Le Roy, K., Opderbecke, J., 2007. Morphology and environment of cold-water coral carbonate mounds on the NW European margin. *International Journal of Earth Sciences* 96, 37–56.
- White, M., Dorschel, B., 2010. The importance of the permanent thermocline to the cold water coral carbonate mound distribution in the NE Atlantic. *Earth and Planetary Science Letters* 296, 395–402.
- White, M., Roberts, J.M., van Weering, T., 2007. Do bottom-intensified diurnal tidal currents shape the alignment of carbonate mounds in the NE Atlantic? *Geophysical Research Letters* 27, 391–397.
- Zimmerman, J.T.F., 1981. Dynamics, diffusion and geomorphological significance of tidal residual eddies. *Nature* 290, 549–555.
- Zimmerman, J.T.F., 1986. The tidal whirlpool: a review of horizontal dispersion by tidal and residual currents. *Netherlands Journal of Sea Research* 20, 133–154.